scientific reports

Check for updates

OPEN

A thermoelectric wristband based on single-walled carbon nanotubes for energy harvesting

Xudong Shen[1,2], Yizhou Qi[1]✉, Mingzhu Yuan[1], Dayi Chen[1], Yiran Wang[1], Yanwei Sun[1] & Ge Shi[1]✉

Single-walled carbon nanotubes (SWCNTs) have attracted increasing attention in wearable thermoelectric devices due to their extremely high strength and toughness. Here we introduce a flexible thermoelectric wearable wristband based on SWCNTs. High-performance SWCNTs films were successfully fabricated through ultrasonic dispersion and heat-pressing processes, exhibiting a Seebeck coefficient of 42.5 μV/K and a maximum electrical conductivity of 3503 S/cm. The flexible films exhibited excellent bending durability, with an impedance increase of no more than 7.6% after 400 bending cycles.The width and length of the thermoelectric legs were optimized, and a wearable thermoelectric wristband was simulated by connecting the legs in series, thereby analyzing its total output power. Furthermore, a thermoelectric wristband was fabricated by spin-coating onto a flexible printed circuit (FPC) substrate, and it achieved a maximum output power of 10.7 μW under a temperature difference of 36.5 K. This research provides an efficient and feasible energy harvesting pathway for utilizing carbon-based materials as thermoelectric materials.

The booming development of flexible electronics technology has significantly promoted the application of wearable electronic devices in daily life. In recent years, the continuous advancement of self-powered technology, with its unique advantage of not requiring external batteries, has become an indispensable and vital component in the wearable technology field[1,2]. Thermoelectric generators (TEGs) efficiently convert thermal energy into electrical energy and are considered as a high-potential pathway for the development of wearable self-powered electronic devices[3]. The skin of the human body possesses a heat dissipation capacity ranging from 100 W to 525 W, rendering it an ideal heat source[4]. However, the development of TEGs that concurrently exhibit high performance, high flexibility, and long-term adaptability to the human micro-environment remains challenging, significantly restricting the widespread adoption of wearable self-powered electronic devices[5].

Thermoelectric efficiency is commonly evaluated by the ZT value, where $ZT = S^2\sigma T/k$. Here, S, σ, T, and k represent the Seebeck coefficient, electrical conductivity, absolute temperature, and thermal conductivity respectively[6]. Currently, inorganic thermoelectric materials are recognized for their excellent thermoelectric properties, which are attributed to their controllable high electrical conductivity (σ) and notable Seebeck coefficient (S)[7]. However, inorganic materials are plagued by defects such as high cost, significant rigidity, and toxicity, which severely restrict their practical applications, particularly in the field of wearable flexible thermoelectric generators (FTEGs)[8,9]. In contrast, most organic materials, such as conductive polymers, inherently possess low thermal conductivity (k). However, due to their relatively low Seebeck coefficient and the numerous challenges in effectively enhancing it, their power factor ($S^2\sigma$) is also relatively low, resulting in significantly different thermoelectric properties compared to those of inorganic materials[10].

Carbon-based thermoelectric materials have garnered considerable attention in the scientific community due to their excellent flexibility, non-toxicity, low cost, and ease of processing. SWCNTs achieve a relatively high Seebeck coefficient, thanks to their high electrical conductivity (σ reaching 10^2–10^4 S/cm) and unique electronic structure[11]. The high electrical conductivity of SWCNTs stems from the high carrier mobility of their long-range conjugated π-electron system, while the quantum confinement effect and chirality-dependent electronic states further enhance their remarkable Seebeck coefficient. This successfully overcomes the traditional trade-off between electrical conductivity and the Seebeck coefficient observed in conventional materials[12,13]. By optimizing their structure and interface design, SWCNTs pave a new path for self-powered wearable electronic devices in terms of efficiency, flexibility, and environmental performance.

[1]China Jiliang University, Hangzhou 310018, Zhejiang, People's Republic of China. [2]Jiaxing Vocational & Technical College, Jiaxing 314036, Zhejiang, People's Republic of China. ✉email: qiyizhou@cjlu.edu.cn; shige@cjlu.edu.cn

This paper delves into the research on flexible thermoelectric wearable wristbands based on SWCNTs. The main research findings are as follows:

(1) Preparation and optimization of SWCNTs dispersions: We successfully prepared a uniform SWCNTs dispersion containing 0.4 wt% conductive agent and 0.6 wt% dispersant. After 30 min of ultrasonic treatment, a good dispersion was achieved. Test results of the prepared samples demonstrated a maximum thermoelectric coefficient of 42.5 μV/K and a maximum conductivity of 3503 S/cm. Bending tests confirmed the performance stability of the flexible thermoelectric SWCNTs material after multiple bending cycles.
(2) Thermoelectric model simulation and optimization: A three-dimensional model of the FTEGs was established using COMSOL multiphysics software. The performance of a single thermoelectric unit and of 120 thermoelectric units connected in series was simulated and analyzed. By adjusting the external load resistance, the output voltage, current, and power of the thermoelectric wristband were optimized.
(3) Design and fabrication of the FTEGs wearable wristband: A PI FPC board was designed, and the copper electrodes were gold-plated to enhance their conductivity. The SWCNTs dispersion was spin-coated onto the FPC board using a shadow mask, followed by drying and heat-pressing processes that improved the density of the SWCNTs film and its bonding strength to the FPC board.
(4) A temperature-difference-controllable test platform, designed to simulate the human wrist, was constructed to comprehensively evaluate the actual performance of the FTEGs wearable wristband. The results demonstrated excellent thermoelectric conversion efficiency and outstanding mechanical flexibility, achieving a maximum output power of 10.7 μW.

Discussion and results

Preparation and performance analysis of carbon nanotube dispersion

The process for fabricating SWCNTs films is depicted in Fig. 1a, the experimental methods section already provides more detailed experimental steps and conditions. The preparation of SWCNTs films mainly involves three steps: ultrasonic dispersion of SWCNTs in ethanol, spin-coating the dispersion onto the substrate, and heat pressing. Compared with commonly-used methods such as vacuum filtration[14,15] and mold casting[16].

Film formation is accomplished using spin-coating method, which is convenient for batch production. Figure 1b and c show the mixed solution of SWCNTs and the films prepared using the solvent hot pressing method, respectively. Figure 1c shows five strip samples of the film after spin-coating the PI substrate and cutting it for testing. The flexibility of the sample strip is shown on the upper right corner. The functional properties of materials are fundamentally governed by their underlying microstructural features, to investigate this relationship, we performed high-resolution scanning electron microscopy (SEM, Zeiss Gemini 500) characterization combined with elemental mapping to analyze the architectural attributes of the SWCNTs network. Figure 1d shows the microstructural characterization, the SWCNTs exhibit a directionally aligned bundled network, the hot-pressing treatment compacts the SWCNTs film under vertical pressure, reducing its thickness and leading to stacking and overlapping between layers. This architecture reduces electron scattering paths and provides efficient charge transport channels, thereby enhancing electrical conductivity[17,18]. The networked structure critically enables device operation under mechanical deformation: during bending, SWCNTs undergo reversible sliding rather than fracture, resulting in minimal resistance fluctuation, this ensures operational stability during wearable use (e.g., limb movement). Figure 1e shows the C-element Mapping, carbon is uniformly distributed without aggregation, confirming the continuity of conductive pathways essential for forming an interconnected network[11].

To elucidate the impact of heating and press temperature of SWCNTs, five temperature points within the range of 60–140 °C were chosen for hot-pressing to prepare the samples (S-60 to S-140). Figure 1f shows the testing platform for SWCNTs films was self-made using Peltier cooling elements. As illustrated in Fig. 1g,h, with an increasing temperature, the S of the SWCNT film changes gently, the maximum difference is only between 2 and 3 μV/K, with a maximum thermoelectric coefficient reaching 42.5 μV/K, the results indicate the thermal properties of the material exhibit high stability at different temperatures. However, the electrical conductivity exhibits significant differences at different temperatures, with a maximum conductivity of 3503 S/cm obtained after heat pressing at 100 ℃, this trend is consistent with the findings of Li et al.[15]. The reason may be that high temperatures can cause partial brittleness and fracture of the carbon nanotube structure, while low temperatures may affect the effective connections between the carbon nanotubes.

To evaluate the performance stability of flexible thermoelectric carbon nanotube materials after multiple bending cycles, a simple bending test platform was constructed, with the bending span adjustable from 5 mm to 15 mm, as shown in Fig. 1i, after bending 400 times, the resistance of the sample(S-100) increase no more than 7.6%, this trend is consistent with the findings of Jin et al.[7], and there were no obvious defects and cracks on the film surface, this fully demonstrates the excellent performance stability of the material under bending conditions.

Theoretical analysis and simulation of flexible thermoelectric wristbands

The calculation of open-circuit voltage (V_{oc}) and output power (P) for SWCNTs FTEGs with multiple legs can be systematically derived from key parameters, such as the Seebeck coefficient (S) and electrical conductivity (σ).

(1) Calculation of open-circuit voltage (V_{oc})

Open-circuit voltage refers to the potential difference generated by a temperature gradient in a thermoelectric material under open-circuit conditions. For a FTEGs composed of n thermoelectric legs connected in series, its open-circuit voltage V_{oc} can be expressed as Eq. (1):

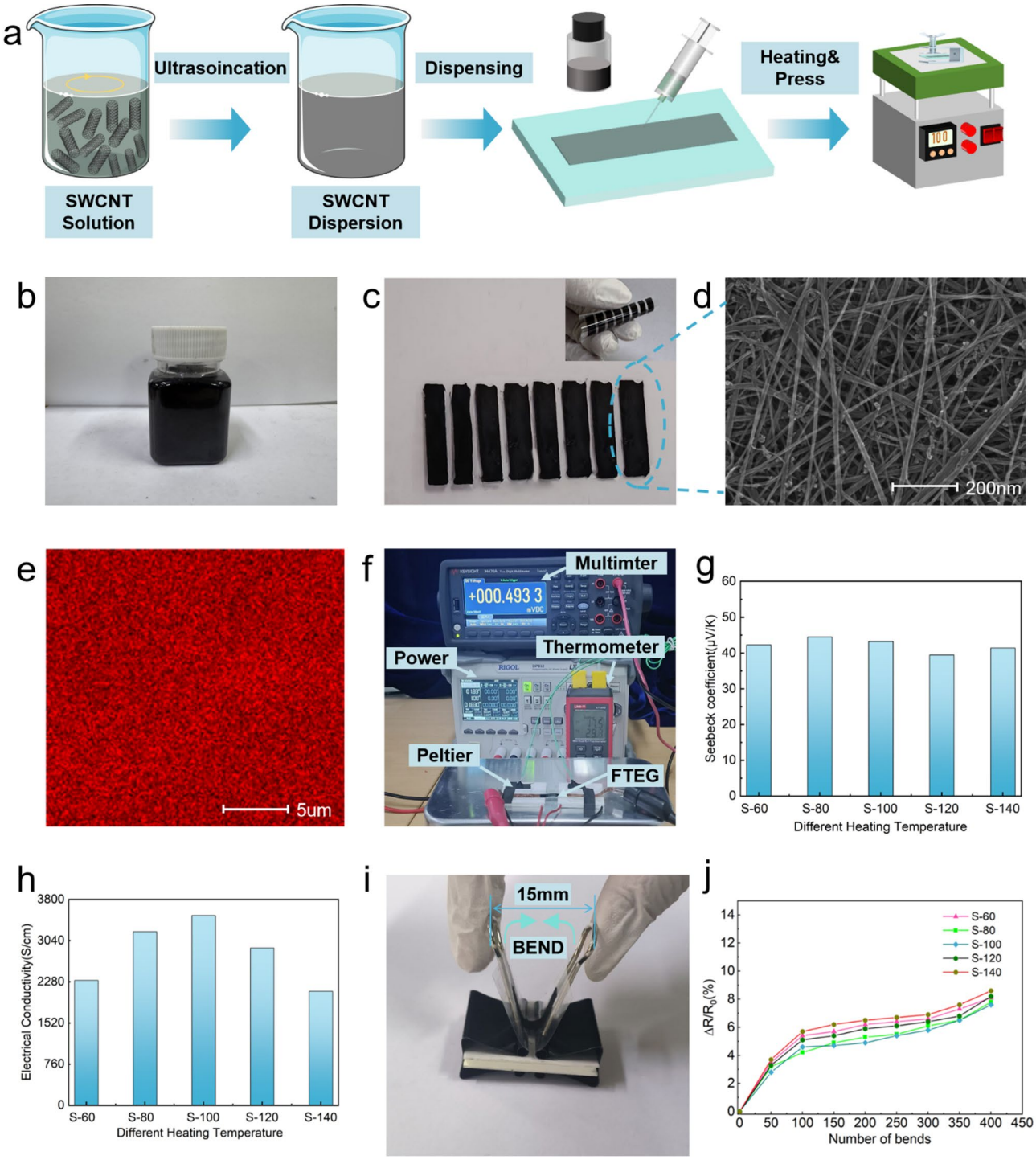

Fig. 1. (**a**) Synthesis process and characterization methods of carbon nanotube film. (**b**) Self-prepared carbon nanotube dispersion solution. (**c**) Flexible thermoelectric film fabricated via conventional process. (**d**) SEM image of strip-shaped thermoelectric film sample. (**e**) Elemental mapping of SWCNTs thin films. (**f**) Custom-built testing platform for thermoelectric films. (**g**) Temperature-dependent variation of Seebeck coefficient. (**h**) Temperature-dependent electrical conductivity. (**i**) Bending test experiment. (**j**) Resistance variation of samples under different bending cycles.

$$V_{oc} = n \cdot s \cdot \Delta T \tag{1}$$

where S is the Seebeck coefficient, a crucial parameter describing the material's thermoelectric conversion capability, representing the potential difference generated per unit temperature gradient. ΔT is the temperature difference between the two ends of the thermoelectric leg.

(2) Calculation of internal resistance (*R*).

Internal resistance R includes the internal resistance of the thermoelectric legs and contact resistances among others. To simplify the calculation, we assume that all thermoelectric legs have the same internal resistance and that contact resistances are negligible. In this case, the internal resistance R_{leg} of each thermoelectric leg can be expressed as Eq. (2):

$$R_{leg} = \frac{L}{\sigma \cdot A} \tag{2}$$

where σ is the electrical conductivity, and A is the cross-sectional area. Since the n thermoelectric legs are connected in series, the total internal resistance R of the thermoelectric generator can be expressed as Eq. (3):

$$R = n * R_{leg} = \frac{n \cdot L}{\sigma \cdot A} \tag{3}$$

(3) Calculation of output power (*P*).

Output power refers to the ability of a thermoelectric generator to convert thermal energy into electrical energy under actual working conditions. For an FTEGs composed of n thermoelectric legs connected in series, its maximum output power *P* can be expressed as Eq. (4):

$$P = \left(\frac{V_{oc}}{2}\right)^2 \cdot \frac{1}{R} \tag{4}$$

where R is the internal resistance of the thermoelectric generator, including the internal resistances of the thermoelectric legs and contact resistances, among others. To simplify the calculation, we assume that all thermoelectric legs have the same internal resistance and that contact resistances are negligible.

By substituting the expressions for V_{oc} and *R* into the above equation, we obtain Eq. (5):

$$P = \left(\frac{n \cdot s \cdot \Delta T}{2}\right)^2 \cdot \frac{\sigma \cdot A}{n \cdot L} \tag{5}$$

After simplification, we get Eq. (6):

$$P = \frac{n \cdot s^2 \cdot \sigma \cdot A \cdot (\Delta T)^2}{4L} \tag{6}$$

We conducted an in-depth investigation into the influence of thermoelectric leg width on the V_{OC}, by varying the width from 500 μm to 3.5 mm. With the leg length maintained constant at 20 millimeters, a hot-side temperature of 309.65 K was applied, while the cold side was subjected to natural convection at an ambient temperature of 293.15 K. The thermal conductivity coefficient, h, was set at 25 W/m^2·K. We observed the maximum V_{OC} for the thermoelectric legs. The V_{OC} output magnitudes across different leg widths are illustrated in Fig. 2a. The width variation within the range of 0.5–3.5 mm exerted a negligible influence on V_{OC} output. This observation aligns with the findings reported by Milad et al.[19] while the V_{OC} output initially increases sharply and subsequently declines across a broader width spectrum (10 μm–10 mm), it reaches its peak and maintains stability within the 0.5–3.5 mm range. However, under constant electrical conductivity conditions, the width of the thermoelectric leg is inversely proportional to its resistance, meaning narrower legs exhibit higher resistance. Considering these factors and prioritizing ease of fabrication, a thermoelectric leg width of 3 mm was selected for this study.

Furthermore, we examined the effect of altering the thermoelectric leg length on V_{OC} within a range of 5 to 80 mm. As depicted in Fig. 2b, an increase in thermoelectric leg length led to an elevation in V_{OC}. Notably, when the thermoelectric leg length exceeded a certain threshold (approximately 20 mm), the V_{OC} began to approach a saturation point of 0.23 mV. Although the V_{OC} output continued to increase with leg length, the rate of increase became progressively flatter, which is consistent with the findings of Milad et al.[19]. Given a constant electrical conductivity, the length is directly proportional to the resistance of the thermoelectric leg. Selecting a leg length close to this optimal value achieves the desired V_{OC} without the need for further elongation to maximize the performance of the thermoelectric leg. This approach not only ensures efficient energy harvesting, but also aids in maintaining the overall flexibility and wearability of the device at the optimal thermoelectric leg length. In this study, we selected a thermoelectric leg length of 20 mm.

To delve deeper into the power generation performance of the FTEGs wristband, we constructed an FTEGs simulation model in COMSOL multiphysics software. Traditionally, thermoelectric generators have employed inorganic materials such as Bi_2Te_3 and PbTe, with their hot and cold ends typically designed at the two terminals of the device to generate voltage by controlling the temperature difference[4,20]. However, due to the small size of the thermoelectric device, the significant thermal conduction effect causes the temperatures at the two ends of the device to quickly converge, thereby affecting the output voltage. To address this, we adopted organic flexible thermoelectric materials, designed the thermoelectric legs in an elongated shape, and integrated the thermoelectric wristband on both sides of a PI substrate by sharing a common cold end. The simulation results revealed that, at a temperature difference of 36.5 K, the temperature distribution of the FTEGs is shown in Fig. 2c, where the purple area represents the low-temperature zone and the orange-yellow area represents the high-temperature zone. Furthermore, we simulated the variation of the FTEGs's output voltage and power with

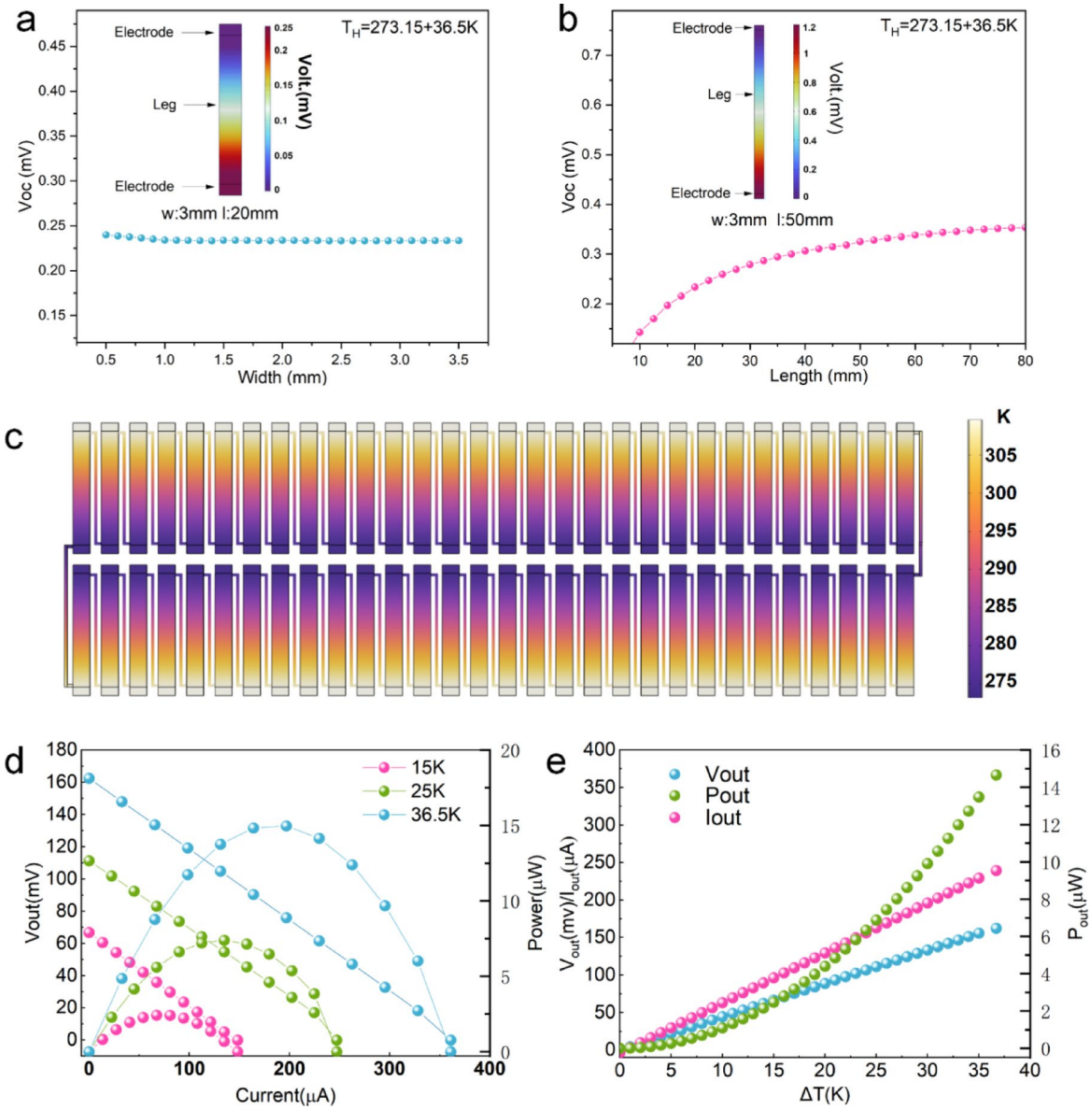

Fig. 2. (**a**) The influence of thermoelectric leg width on open-circuit voltage. (**b**) The influence of thermoelectric leg width on open-circuit voltage. (**c**) Temperature distribution of the thermoelectric wristband at ΔT of 36.5 K. (**d**) Relationship between voltage, power, and current in the FTEGs under different temperature gradients(15 K, 25 K, 36.5 K). (**e**) Power, voltage, and current generated by the FTEGs under different temperature differences.

output current under different temperature differences, as illustrated in Fig. 2d, based on changes in the external load. Under conditions of a temperature difference of 36.5 K and 120 thermoelectric legs, the maximum output power of the FTEGs reached 14.96 μW (as shown in Fig. 2e) which is sufficient to meet the power requirements of general low-power consumption products.

The fabrication and performance testing of the FTEGs wristband

Figure 3a shows the as-fabricated FTEGs consists of three parts, the middle section is FTEGs part, and the exterior is covered with a transparent Polydimethylsiloxane (PDMS) protective layer. FTEGs part includes 120 SWCNTs legs, and it is the most critical component that converts thermal energy into electrical energy. The design of PDMS not only enhances the durability of the wristband, but also ensures the stability of the thermoelectric conversion process. The upper right corner photo shows the convenient wearing method of the FTEGs thermoelectric wristband, proving its potential in practical applications.

During the preparation of the wristband, we used a flexible FPC board made of PI material to ensure the reliability of the process. To ensure a reliable connection between SWCNTs and the electrodes, we applied a gold immersion process to the electrodes. Compared to the manual application of silver paste method adopted by Hong et al.[21]our gold immersion process on the FPC board substrate significantly improves the

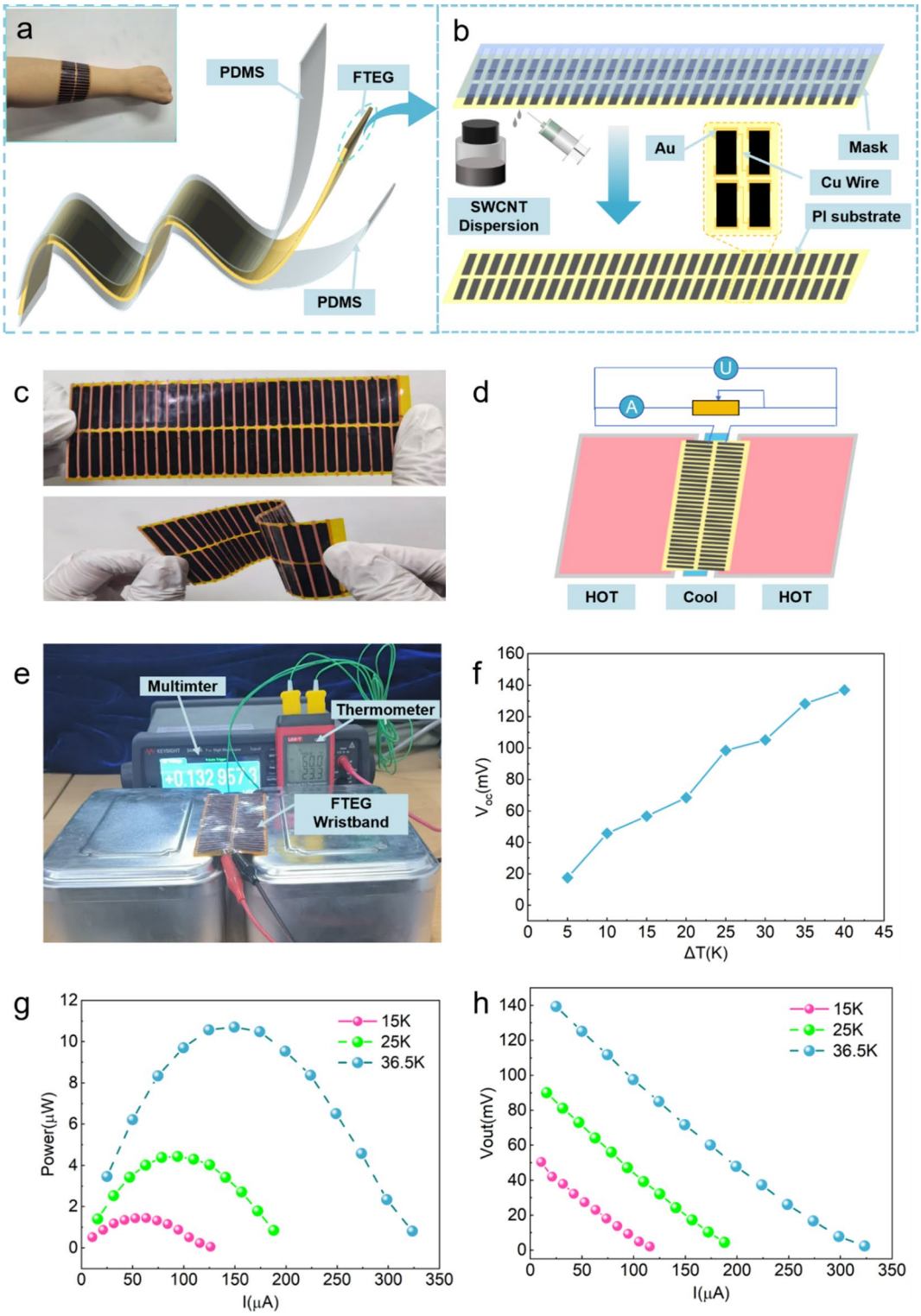

Fig. 3. (**a**) Schematic diagram of the structure of the FTEGs wristband. (**b**) The fabrication progress of the FTEGs wristband. (**c**) Photo of the FTEGs wristband. (**d**) Schematic diagram of the testing platform for the FTEGs wristband. (**e**) Photo of testing platform for the FTEGs wristband. (**f**) Relationship between open-circuit output voltage and temperature difference. (**g**) Relationship between output power and output current. (**h**) Relationship between output voltage and output current.

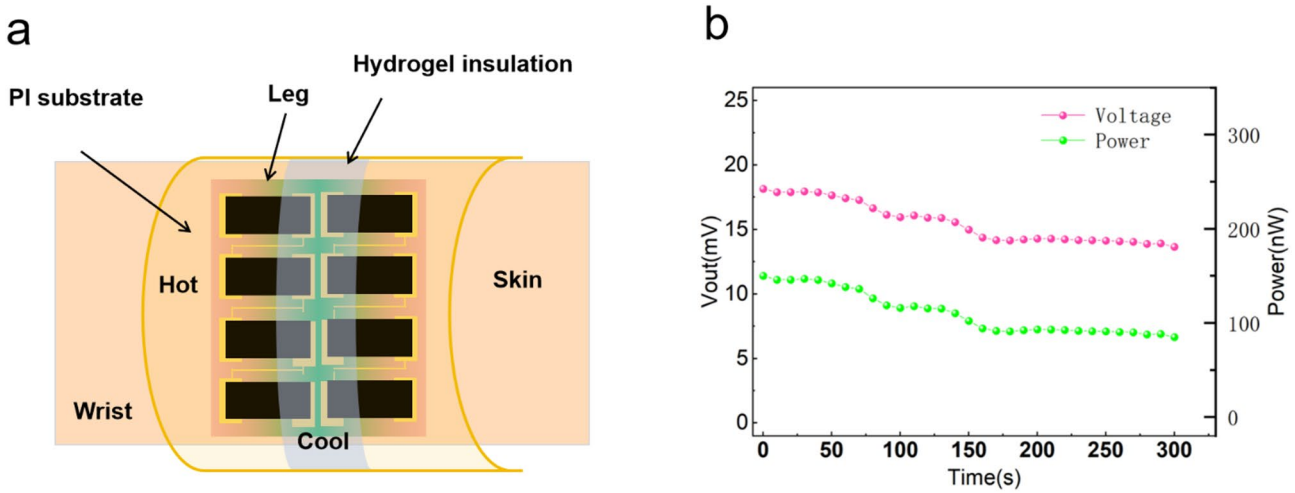

Fig. 4. (**a**) Demonstration of the FTEGs wristband wearing method and its human body thermal energy harvesting process. (**b**) The performance of power generation using human body thermal energy at a temperature difference of 5 K.

manufacturing efficiency and reliability of the wristband. The traditional manual method of connecting wires is prone to fractures at the junctions of the two materials, especially when there are numerous thermoelectric legs, which can easily lead to instability of the thermoelectric wristband. As illustrated in Fig. 3b, before spin coating, a meticulously designed mask plate was affixed onto the FPC board. Subsequently, the carbon nanotube dispersion solution prepared earlier was uniformly applied onto the substrate via spin coating, and after drying and heat-pressing processes, the initial preparation of the thermoelectric wristband was completed, compared to the method of fabricating thermoelectric films from carbon nanotubes, cutting them into strips, and connecting them in series[11]. This approach enables the rapid fabrication of thermoelectric wristbands. Figure 3c shows the photo of the SWCNTs-based FTEGs, and excellent flexibility of FTEGs can be seen.

To assess the performance of the FTEGs in a practical application, we constructed a flexible thermoelectric test platform, the schematic diagram of the platform is shown in Fig. 3d. The actual test platform under different temperature differences is shown in Fig. 3e, the platform device employs thermally conductive aluminum boxes on both sides of the thermoelectric wristband, and specific temperature water is added for testing, the middle part of the wristband serves as the cold end, where a hydrogel patch is used for cooling control to ensure a temperature difference between the hot and cold ends. As illustrated in Fig. 3f, the thermoelectric coefficient of the FTEGs wristband at 313.15 K is 137.07 mV. Although this result is slightly lower than the simulation expectations, it is attributed to the inherent thermal conductivity of the carbon nanotubes during the actual testing process. Additionally, we analyzed the relationship between the output voltage and output current (as shown in Fig. 3g, and tested the variation of output power with output current at different temperatures (as shown in Fig. 3h), the results indicated that the maximum output power reached 10.7 uW, the FTEGs wristband demonstrated stable thermoelectric conversion performance.

In addition, we employed the fabricated thermoelectric wristband to harvest human body thermal energy. Figure 4a clearly demonstrates the wearing method of the FTEGs thermoelectric wristband and elaborates on its working mechanism for collecting thermal energy from the human body. Specifically, the human skin serves as the heat source, and a hydrogel is used in the middle of the wristband for insulation and heat dissipation. We placed the wristband on the wrist of a subject and tested its output performance under the condition where there was a 5 K temperature difference between the ambient temperature and the human skin temperature. The test results are shown in Fig. 4b, the initial open-circuit voltage is 18.15 mV, and an output power of 150.06 nW is achieved under a 510Ω load. As time progresses, both the open-circuit voltage and the output power experience a slight decline, this is primarily due to the reduction in the temperature difference between the two ends caused by heat conduction[21,22].

Methods

Preparation of carbon nanotube dispersions

SWCNTs and PVP (polyvinylpyrrolidone) dispersant were purchased from Suqian NCT Materials Co., Ltd. A solution was prepared by dissolving 0.2 g of SWCNTs and 0.3 g of PVP dispersant in 50 milliliters of deionized water. The mixture was stirred at 300 rpm for 2 h, yielding a uniform dispersion with a conductive agent content of 0.4 wt% and a dispersant content of 0.6 wt%. Subsequently, the dispersion underwent ultrasonic treatment in an ice bath for 30 min to prevent changes due to overheating during the ultrasonication process. Finally, the processed carbon nanotube dispersion was stored in a suitable container. Then, a certain amount of the dispersion was drawn using a syringe and spin-coated onto a PI substrate with dimensions of 20 mm by 5 mm. During the spin-coating process, care was taken to ensure uniform thickness. The coated substrate was subsequently dried on a heating plate at 100 °C for 1 h and then subjected to a vertical pressure of 2 MPa using a press for 10 min.

Simulation of thermoelectric models

A three-dimensional model of the FTEGs was created utilizing COMSOL Multiphysics 6.1, which can be accessed at https://www.comsol.com. Initially, the performance of a single thermoelectric element was tested within the COMSOL multiphysics environment. Subsequently, 120 Legs were integrated in series, and steady-state simulations were conducted using the thermoelectric effect and circuit modules. Circuit nodes were utilized to connect the ammeter, external load, FTEGs, and voltmeter, thus constructing the circuit simulation model. By varying the resistance of the external load, data were collected from the ammeter and voltmeter.

Design of the FTEGs-based wearable wristband

Based on the simulation results, we designed a FPC board made of PI material and applied gold plating to the copper electrodes to enhance their conductivity. To ensure better spin-coating results and improve efficiency, we first designed a mask and placed it over the FPC board. The SWCNTs dispersion was then applied to the FPC board using a syringe for spin-coating, ensuring a uniform coating to avoid thickness variations. The coated FPC board was subsequently placed in an oven and dried at 100 °C for 1 h. After drying, the FPC board was subjected to heat-pressing with a vertical pressure of 2 MPa for 10 min to enhance the density of the SWCNTs film and to ensure tight bonding with the flexible FPC board.

Performance evaluation of the FTEGs wearable wristband

To evaluate the performance and practical application of the FTEGs wearable wristband, a temperature-difference-controllable test platform was established. A thermally conductive aluminum box filled with water at a specific temperature was utilized. The FTEGs wearable wristband was then tightly attached to the outer sides of the aluminum box, while a hydrogel was applied to the middle section of the wristband to serve as the cold end for thermal insulation and cooling. Temperature data were collected using a UNI-T contact thermometer probe. By controlling the temperature, the actual performance of the device was measured. The FTEGs wearable wristband was tested with external resistors of different values, and the relationships between voltage, current, and output power were recorded by varying the external load resistance. During the performance testing, the measured data were processed to calculate both the mean and variance, as shown in Eqs. (7) and (8). Therefore, each data point in the graphs represents the average of the measured data, and a smaller variance indicates that the data set deviates less from the mean, making the data more reliable[3].

$$\mu = \frac{x_1 + x_2 + \cdots x_n}{n} \tag{7}$$

$$\delta = \sqrt{\frac{1}{n}\sum\nolimits_{i=1}^{n}(x_i - \mu)^2} \tag{8}$$

Conclusion

In this study, we presented a FTEGs wearable wristband based on SWCNTs. Through a meticulous fabrication process, a uniformly dispersed carbon nanotube film with excellent electrical conductivity was obtained. Utilizing COMSOL Multiphysics for simulation and optimization, the thermoelectric wristband demonstrated promising thermoelectric conversion performance. By fabricating a thermoelectric wristband and conducting tests, it was shown that the maximum output power of the wristband reached 10.7 μW at a temperature difference of 36.5 K. This thermoelectric wristband proposes an effective solution in the field of carbon-based thermoelectric wearable devices. Future research will focus on further optimizing the material composition and device structural design, aiming to enhance the output power and improve long-term durability.

Data availability

The data supporting the plots in this paper are available from the corresponding author upon reasonable request.

Received: 19 March 2025; Accepted: 18 July 2025
Published online: 23 July 2025

References

1. Van Toan, N., Tuoi, K., Ono, T. & T. T. & High-performance flexible thermoelectric generator for self-powered wireless BLE sensing systems. *J. Power Sources*. **536**, 231504 (2022).
2. Yuan, J. & Zhu, R. A fully self-powered wearable monitoring system with systematically optimized flexible thermoelectric generator. *Appl. Energy*. **271**, 115250 (2020).
3. Yang, S. et al. Flexible thermoelectric generator and energy management electronics powered by body heat. *Microsyst. Nanoeng.* **9**, 106 (2023).
4. Jin, J. et al. High-performance waterproof flexible thermoelectric generators for self-powered electronics. *Nano Energy*. **132**, 110388 (2024).
5. Chen, W. et al. Nanobinders advance screen-printed flexible thermoelectrics. *Science* **386**, 1265–1271 (2024).
6. Zheng, Z. H. et al. Harvesting waste heat with flexible Bi2Te3 thermoelectric thin film. *Nat. Sustain.* **6**, 180–191 (2022).
7. Jin, Q. et al. Flexible layer-structured Bi2Te3 thermoelectric on a carbon nanotube scaffold. *Nat. Mater.* **18**, 62–68 (2019).
8. Tan, G., Zhao, L. D. & Kanatzidis, M. G. Rationally designing high-performance bulk thermoelectric materials. *Chem. Rev.* **116**, 12123–12149 (2016).
9. Yang, L., Chen, Z., Dargusch, M. S. & Zou, J. High performance thermoelectric materials: progress and their applications. *Adv. Energy Mater.* **8**, 1701797 (2018).
10. Kim, W. S. et al. Feasible tuning of barrier energy in PEDOT:PSS/Bi2Te3 nanowires-based thermoelectric nanocomposite thin films through Polar solvent vapor annealing. *Nano Energy*. **67**, 104207 (2020).

11. Liu, Y. M. et al. Boosting thermoelectric performance of single-walled carbon nanotubes-based films through rational triple treatments. *Nat. Commun.* **15**, 3426 (2024).
12. Hung, T., Nugraha, N. R. T., Saito, R. & A. & Thermoelectric properties of carbon nanotubes. *Energies*. **12**, 4561 (2019).
13. Hayashi, D. et al. Thermoelectric properties of single-wall carbon nanotube networks. *Jpn. J. Appl. Phys.* **58**, 075003 (2019).
14. Jiang, Q. et al. High-performance hybrid organic thermoelectric swnts/pedot:pss thin-films for energy harvesting. *Mater. Chem. Front.* **2**, 679–685 (2018).
15. Li, L. et al. Flexible thermoelectric films based on Bi_2 Te_3 nanowires and Boron nitride nanotube networks with carbon doping. *ACS Appl. Mater. Interfaces*. **15**, 31812–31823 (2023).
16. Li, W. et al. High thermoelectric properties of Cu2Te Ag2Te composite with Fe addition and non-stoichiometric Te. *J. Materiomics*. **10**, 37–44 (2024).
17. Zhao, K. et al. Enhanced thermoelectric performance of Bi2Te3 by carbon nanotubes and silicate aerogel co-doping toward ocean energy harvesting. *Mater. Today Sustain.* **23**, 100476 (2023).
18. Komatsu, N. et al. Macroscopic weavable fibers of carbon nanotubes with giant thermoelectric power factor. *Nat. Commun.* **12**, (2021).
19. Jabri, M., Masoumi, S., Kandukuri, T. R. & Occhipinti, L. G. Flexible thin-film thermoelectric generators for human skin-heat harvesting: A numerical study. *Nano Energy*. **129**, 110001 (2024).
20. Waktole, D. A. Integration of tau-shaped fins and perforated polyimide substrate for enhanced power output in flexible thermoelectric generator for human body heat harvesting. (2025).
21. Hong, M. et al. Advances in printing techniques for thermoelectric materials and devices. *Soft Sci.* **3**, (2023).
22. Chiba, T., Amma, Y. & Takashiri, M. Heat source free water floating carbon nanotube thermoelectric generators. *Sci. Rep.* **11**, (2021).

Acknowledgements

This research is supported by the National Natural Science Foundation of China, China under Grant 62334006, Grant 62271275, Grant 62131010 and Grant U22A2013 in part by the Zhejiang Provincial Natural Science Foundation of China, China under Grant LR22F010001, the Project of Scientific and Technological Plan of Zhejiang Province, China under Grant 2024C01, and the Project of Jiaxing Science and Technology, Grant 2023AY11027,Project of the Zhejiang Provincial Department of Education, Grant Y202250242.

Author contributions

X.D.S. nvestigation, methodology, writing—original draft, Y.Z.Q., Y.R.W. and Y.W.S. Writing—review and editing, M.Z.Y., D.Y.C. Methodology, G.S. Funding acquisition, methodology, project administration, resources, supervision, writing—review and editing.

Declarations

Competing interests

The authors declare no competing interests.

Additional information

Correspondence and requests for materials should be addressed to Y.Q. or G.S.